# Exciton states and optical properties of CdSe nanocrystals

Jesús Pérez-Conde
*Departamento de Física, Universidad Pública de Navarra, E-31006 Pamplona, Spain*

A. K. Bhattacharjee
*Laboratoire de Physique des Solides, UMR du CNRS, Université Paris-Sud, 91405 Orsay, France*
(Received 18 October 2000; revised manuscript received 17 January 2001; published 6 June 2001)

The optical spectra of CdSe nanocrystals up to 55 Å in diameter are analyzed in a wide range of energies from the fine structure of the low-energy excitations to the so-called high-energy transitions. We apply a symmetry-based method in two steps. First we take the tight-binding (TB) parameters from the bulk $sp^3s^*$ TB model, extended to include the spin-orbit interaction. The full single-particle spectra are obtained from an exact diagonalization by using a group-theoretical treatment. The electron-hole interaction is next introduced: Both the Coulomb (direct) and exchange terms are considered. The high-energy excitonic transitions are studied by computing the electric dipole transition probabilities between single-particle states, while the transition energies are obtained by taking into account the Coulomb interaction. The fine structure of the lowest excitonic states is analyzed by including the electron-hole exchange interaction and the wurtzite crystal-field terms in the exciton Hamiltonian. The latter is diagonalized in the single electron-hole pair excitation subspace of progressively increasing size until convergence. The peaks in the theoretical transition spectra are then used to deduce the resonant and nonresonant Stokes shifts, which are compared with their measured values in photoluminescence experiments. We find that the final results depend on the crystal-field term, the relative size of the surface, and the degree of saturation of the dangling bonds. The results show satisfactory agreement with available experimental data.

DOI: 10.1103/PhysRevB.63.245318 PACS number(s): 73.22.−f, 71.35.Cc, 78.55.−m, 78.66.Hf

## I. INTRODUCTION

The optical properties of semiconductor nanocrystals have attracted considerable attention in recent years due to their possible applications in quantum dot lasers and other devices (see, for example, Ref. 1), and, from a more basic point of view, because the nanocrystals are the physical realization of small systems where the effect of the low dimensionality should be most important. We are interested here in CdSe nanocrystals, which have been intensively studied by several groups.[2–8] The high-energy excitonic transitions have been investigated to some extent,[7,8] but most of the experimental works have been devoted to the study of the size dependence of the photoluminescence and the fine structure of the low-energy exciton states.[3–6] In particular, the observation of the ''dark exciton'' in CdSe quantum dots (QD's) is one of the more salient features.

Several theoretical models have been proposed following two main starting points. First, the ''particle in the box'' point of view is realized in the effective-mass approximation (EMA) used by several groups[3,9] and the effective-bond-orbital model by Laheld and Einevoll.[10] From the other point of view, where the QD electron wave function is explicitly constructed from the atomiclike orbitals, we note the pseudopotential[11,12] and the semiempirical TB[13,14] methods.

The TB model that we present here is particularly suitable for describing small nanocrystals. Comparing to the EMA theories, which are known to be inadequate for the energy gap at small sizes, some surface conditions can be varied continuously and their influence in the final result evaluated. Also, we analyze the many-body exciton Hamiltonian in a controlled way: the electron-hole space is expanded until the convergence in energies is reached. The cited EMA theories, in contrast, use a fixed number of electron-hole states. The pseudopotential calculations published so far[11,12] have been limited to smaller sizes ($D<40$ Å) than ours and some results such as the crystal-field splitting of the valence band seem to be controversial: this splitting is expected to be smaller in QD's than in the bulk.[15]

Finally, the previous TB calculation of the exciton fine structure by Leung, Pockrant, and Whaley[13] is based on an unsatisfactory truncation procedure. These authors first use a Lanczos algorithm to deduce a few orbital (spin-degenerate) single-particle states below and above the energy gap and then introduce the spin-orbit coupling in the restricted subspace used for diagonalizing the exciton Hamiltonian. However, in CdSe nanocrystals, the spin-orbit interaction is almost an order of magnitude larger than the average spacing of the TB single-particle levels and drastically modifies the level scheme. Thus their method seems inappropriate beyond the immediate vicinity of the exciton ground state. In this paper we propose a different approach that allows a rather complete study of the exciton spectrum. It is based on symmetrized single-particle states that are first obtained by an exact diagonalization of the full zinc-blende TB Hamiltonian including the spin-orbit interaction. The relatively small crystal-field term ($\sim \frac{1}{15}$th of the spin-orbit term) representing the wurtzite crystal structure is then diagonalized in the subspace spanning the exciton states. Not surprisingly, we obtain a fine-structure spectrum of the exciton ground state that is quite different from Ref. 13, especially in terms of the relative intensities of the components. Moreover, our study is not limited to the lowest-energy excitations: We present re-

 

TABLE I. Some properties of studied QD's are shown. The first column gives the effective diameter, the second and third show the number of atoms and dangling bonds, respectively. In the last three columns we give the crystal-field splitting (in meV) of the valence band for the different values of Cd-H bond length.

| $D$ (Å) | $N_{\text{at}}$ | $N_{\text{dangling}}$ | 0.81 (Å) | 1.21 (Å) | 1.71 (Å) |
|---|---|---|---|---|---|
| 16.63 | 87 | 76 | 6.7 | 4.3 | 3.1 |
| 23.29 | 239 | 196 | 21.0 | 20.7 | 19.9 |
| 30.28 | 525 | 276 | 16.3 | 13.7 | 6.1 |
| 31.60 | 597 | 324 | 21.0 | 20.6 | 17.6 |
| 40.22 | 1231 | 460 | 18.3 | 15.3 | 8.9 |
| 54.78 | 3109 | 852 | 13.1 | 11.5 | 7.4 |

sults on the nonresonant Stokes shifts and the high-energy excitonic transitions.

This paper is organized as follows. In Sec. II we give a brief description of the TB model, the single-particle states, the exciton Hamiltonian, and its diagonalization. In Sec. III we compare our results with the available experimental data and previous theoretical analyses. Finally, in Sec. IV we summarize the main results and present some concluding remarks.

## II. TIGHT-BINDING DESCRIPTION OF THE EXCITON STATES

We consider spherical zinc-blende crystallites of diameter ranging from 16.63 Å (87 atoms) to 54.78 Å (3109 atoms). In Table I we list some selected crystallite sizes along with their number of atoms and number of dangling bonds. The one-particle states are obtained using the $sp^3s^*$ nearest-neighbor TB model introduced by Vogl, Hjalmarson, and Dow[16] extended here to include the spin-orbit interaction. We take the tight-binding parameters for CdSe from Ref. 17, except for some minor changes all measured in eV: $E_{s,a}=-11.53$, $E_{p,a}=0.53$, $E_{s,c}=1.83$, $E_{p,c}=5.87$, $V_{s,s}=-3.07$, $V_{x,x}=1.8$, $V_{x,y}=4.23$, $V_{s,p}=2.17$, $V_{p,s}=-5.48$, $E_{s*,a}=7.13$, $E_{s*,c}=6.87$, $V_{s*,p}=1.99$, $V_{p,s*}=-3.06$ eV. The spin-orbit couplings are $\lambda_{\text{Se}}=0.1434$ and $\lambda_{\text{Cd}}=0.059$ eV. The dangling bonds are passivated by hydrogen atoms where the H energy level is set to $E_{s,\text{H}}=-3.3$ eV following the scaling prescription given by Kobayashi, Sankey, and Dow.[18] We assume that the hopping integrals between the anion or cation and hydrogen follow the Harrison scaling rule: $V_{b\text{-H}}=(d_{a\text{-}c}/d_{b\text{-H}})^2V_{ac}$, where the $d_{b\text{-H}}$ are the bond lengths, with $b$ denoting the cation ($b=c$) or anion ($b=a$). The degree of saturation of the dangling bonds is controlled by varying these bond lengths.

We follow a symmetry-based method developed previously[19] to obtain the one-particle states. These are computed by diagonalizing the Hamiltonian built in a block-diagonal form, in terms of the symmetrized basis corresponding to the $\Gamma_6$, $\Gamma_7$, and $\Gamma_8$ double-valued representations of $T_d$. This method allows us to obtain the complete one-particle spectra. The eigenstates can be written as

$$\phi_i=\sum_{R,k,m} C^i_{R,k,m}u^k_m(\mathbf{r}-\mathbf{R}), \tag{1}$$

where we have omitted $b$ and the symmetry label of the eigenstate for brevity. The $u^k_m(\mathbf{r})$ are the spin-orbit coupled atomic orbitals, following the notation by Koster *et al.*[20] They are constructed from the direct product of the standard basis $\{s,s^*,p_x,p_y,p_z\}$ and the electron spin states, all referred to the $\langle 001\rangle$ cubic axis. The $s,s^*$ orbitals transform as $\Gamma_1$, the $p$ orbitals as $\Gamma_5$, and the spin functions as $\Gamma_6$ representations of $T_d$. The resulting spin-orbit coupled orbitals are thus given by $k=\Gamma_6$, $\Gamma_6^*$, $\Gamma_7$, and $\Gamma_8$. There are two sets corresponding to Cd and Se. The subscript $m$ is the row index and $\mathbf{R}$ denotes the atomic site.

Surface effects can be important in nanocrystals, as pointed out previously.[10,19] So, we have analyzed here three different cases of dangling bond saturation. First we take the bond lengths $d_{\text{Cd-H}}=1.71$ Å and $d_{\text{Se-H}}=1.47$ Å, which correspond to the sum of the covalent radii. The analysis of the density of states indicates that there is a relatively important presence of surface states near the band edges as in the case of CdTe quantum dots.[19] The second series is given for $d_{\text{Cd-H}}=1.21$ Å and $d_{\text{Se-H}}=0.97$ Å. In this case the surface contribution has partially disappeared from the states of physical interest. The last series of data correspond to $d_{\text{Cd-H}}=0.81$ Å and $d_{\text{Se-H}}=0.57$ Å, here the contribution of the surface states can be found several electron volts away from the band gap. From these results one can assume that the shortening of the $d_{b\text{-H}}$ can be thought as equivalent to projecting out the surface states from the Hilbert space near the band edge. The physical consequences of the dangling-bond saturation are also equivalent to the method followed in previous TB approaches where the dangling bonds were explicitly removed.[13,21] Therefore, we can consider the atom-hydrogen bond length as an additional fitting parameter. The study of the excitonic structure has been restricted to the last series because the final results seem to be the closest to the measured values. Another surface effect, the surface-to-volume ratio, is considered through the number of dangling bonds relative to the total number of atoms (cations and anions). In Fig. 1 the distribution of the fraction $v=N_{\text{at}}/N_{\text{dangling}}$ is shown, the QD sizes analyzed in this paper are identified by closed squares. Some properties, such as the crystal-field splitting of the valence band edge and the photoluminescence Stokes shifts seem to be very sensitive to the relative number of dangling bonds.

In Table II we show the size dependence of the one-particle energies and the corresponding symmetries of the three highest valence states for the case $d_{\text{Cd-H}}=0.81$ and $d_{\text{Se-H}}=0.57$ Å. It can be seen that the two highest levels are close in energy to each other and well separated from the rest of the band for any size. It is interesting to note that this level scheme near the ''band edge'' fits in with the results of the multiband EMA calculation by Richard *et al.*[22] showing the nearly degenerate quadruplets $1SDD_{3/2}$ and $1PFP_{3/2}$. Notice, however, that neither of our TB $\Gamma_8$ quadruplets is dipole forbidden (see Ref. 19). This energy separation of the two fourfold levels from the rest of the band is important. In fact,

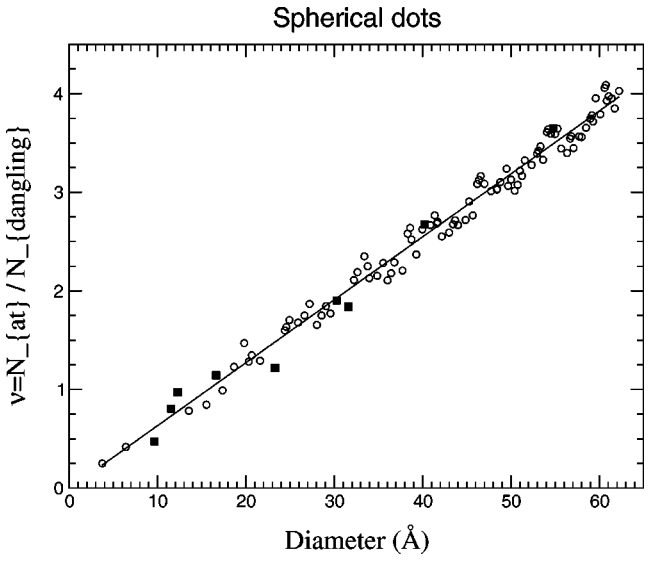


FIG. 1. Ratio of the number of semiconductor atoms and the number of dangling bonds (open circles). The line is the least square linear approximation. The QD's studied in this article are shown by closed squares.

our numerical results for the low-energy exciton states, to be presented later, indicate that the restricted $e$-$h$ subspace spanned by these two highest valence and the lowest conduction levels yields almost the same results as larger subspaces.

The actual crystal structure of the CdSe crystallites is wurtzite.[2,4] This is taken into account as usual by introducing an axial crystal field along a trigonal direction $\langle 111\rangle$ of the zinc-blende nanocrystal. This crystal field splits the atomic $p$ level. In the standard $sp^3s^*$ basis an energy shift has been applied to the $p_z$ orbitals.[13] In our spin-orbit coupled atomic basis the crystal-field Hamiltonian leads to a splitting of the atomic $u_{m_e}^{\Gamma_8}(\mathbf{r})$ energy level into two doublets of $C_{3v}$ symmetry. The corresponding local operator can be written as

$$H_{cf}^{s}=\frac{D}{3}(J_n^2-\tfrac{5}{4})=\frac{D}{3\sqrt{3}}\begin{bmatrix} 0 & -1-i & i & 0 \\ -1+i & 0 & 0 & i \\ -i & 0 & 0 & 1+i \\ 0 & -i & 1-i & 0 \end{bmatrix}, \tag{2}$$

TABLE II. Values of the three highest valence levels (in eV) for different sizes. The symmetry is also written in parentheses. The number in parenthesis 8 (6) is short for $\Gamma_8$ ($\Gamma_6$).

| Diameter (Å) | $v_1$ | $v_2$ | $v_3$ |
|---|---|---|---|
| 16.63 | −1.034(8) | −1.055(8) | −1.163(6) |
| 23.29 | −0.587(8) | −0.672(8) | −0.834(6) |
| 30.28 | −0.436(8) | −0.453(8) | −0.601(6) |
| 31.60 | −0.380(8) | −0.413(8) | −0.578(6) |
| 40.22 | −0.264(8) | −0.277(8) | −0.408(8) |
| 54.78 | −0.158(8) | −0.165(8) | −0.248(8) |

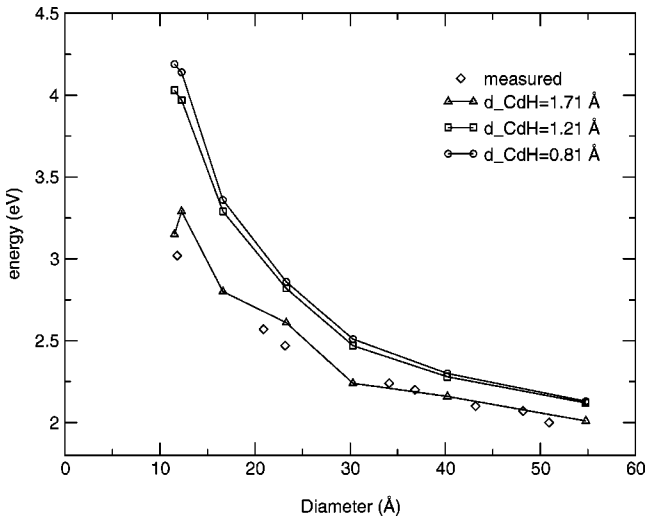


FIG. 2. The calculated excitonic gap vs QD diameter is compared with the experimental data from Ref. 2 (diamonds). The three theoretical curves correspond to different degrees of saturation of the dangling bonds, represented by three different sets of cation- and anion-to-hydrogen bond lengths (see text).

with $D=0.04$ eV and $J_n$ the total angular momentum in the $\langle 111\rangle$ direction, $J_n=(1/\sqrt{3})(J_x+J_y+J_z)$. This value reproduces the crystal-field splitting of the bulk valence band. The matrix elements of $J_x$, $J_y$, and $J_z$ are obtained in the $u_m^{\Gamma_8}$ basis in the standard way.[23] We take the relation between the total angular momentum basis $|JM\rangle$ and the $u_m^{\Gamma_8}$ from Ref. 24.

In the basis of the zinc-blende one-particle states in Eq. (1) a matrix element of the total crystal-field (CF) Hamiltonian is given by

$$\langle\phi_i|H_{\mathrm{CF}}|\phi_j\rangle=\sum_{R,m,n}(C_{R,\Gamma^s,m}^{i})^{*}C_{R,\Gamma^s,n}^{j} \times\langle u_m^{\Gamma^s}(\mathbf{r}-\mathbf{R})|H_{\mathrm{CF}}^{\mathrm{at}}|u_n^{\Gamma^s}(\mathbf{r}-\mathbf{R})\rangle, \tag{3}$$

where $\langle u_m^{\Gamma^8}(\mathbf{r}-\mathbf{R})|H_{\mathrm{CF}}^{\mathrm{at}}|u_n^{\Gamma^8}(\mathbf{r}-\mathbf{R})\rangle$ are the matrix elements of the local crystal-field Hamiltonian in Eq. (2).

To summarize, the total single-particle Hamiltonian that we use is

$$H_{\mathrm{single}}=H_0+H_{\mathrm{CF}}, \tag{4}$$

where $H_{\mathrm{CF}}$ is given in Eq. (3) and $H_0$ is the zinc-blende TB Hamiltonian including the spin-orbit interaction. In order to calculate the crystal-field splitting, $\Delta_{\mathrm{CF}}$, of the highest valence band level we diagonalize $H_{\mathrm{single}}$ in the subspace of a sufficiently large number of valence states of $H_0$ to reach convergence. The results for several surface conditions are given in Table I, where it can be seen that the crystal-field splitting presents an irregular behavior as a function of the QD size. We find that this behavior is related to the relative number of dangling bonds (see Fig. 1). In Table I we can see that for a given QD size the splitting increases when the hydrogen-atom bond length decreases. The same is true of the excitonic band gap shown in Fig. 2. This kind of behavior related to the surface is also found in the exciton fine

structure, even if the nonmonotonic jumps are not so remarkable as for the crystal-field splitting.

A complete description of the elementary excitations is made by introducing the Coulomb interaction between electron and hole. Let us first define the two-particle states needed to describe the excitations above what we call the ground state $|g\rangle$, describing the fully occupied valence band. An electron-hole state can be thought of as the pair obtained when one electron from the valence band is excited above the gap. The effective hole and electron interact through the Coulomb interaction so that we need to describe the excitation in terms of electron-hole pairs. We call these excited states excitons because they describe the same Hilbert state as the bulk excitons when the QD size reaches the thermodynamic limit. These exciton states can be formally written as

$$|e\rangle = \sum_{v,c} C_{v,c}|v,c\rangle, \tag{5}$$

where

$$|v,c\rangle = a_c^\dagger a_v|g\rangle, \tag{6}$$

where the $a_c^\dagger$ ($a_v$) is the creation (annihilation) operator for a conduction (valence) electron and $|g\rangle$ is the many-particle ground state. When the Coulomb interaction is introduced the matrix elements of the total Hamiltonian can be written in the electron-hole basis after some algebra as

$$H_{vc,v'c'} = (\varepsilon_c - \varepsilon_v)\delta_{vv'}\delta_{cc'} - J_{vc,v'c'} + K_{vc,v'c'}, \tag{7}$$

with

$$J_{vc,v'c'} = \left\langle \phi_c(1)\phi_{v'}(2)\left|\frac{V(\mathbf{r}-\mathbf{r}')}{\epsilon(\mathbf{r}-\mathbf{r}')}\right|\phi_v(2)\phi_{c'}(1)\right\rangle, \tag{8}$$

$$K_{vc,v'c'} = \left\langle \phi_{v'}(1)\phi_c(2)\left|\frac{V(\mathbf{r}-\mathbf{r}')}{\epsilon(\mathbf{r}-\mathbf{r}')}\right|\phi_v(2)\phi_{c'}(1)\right\rangle, \tag{9}$$

where the $\phi_{v(c)}$ are given in Eq. (1), $V(\mathbf{r}-\mathbf{r}')$ is the bare Coulomb interaction and we have explicitly included the dielectric constant $\epsilon(\mathbf{r}-\mathbf{r}')$. In the preceding expressions it is implicitly understood that we consider only excitations involving a single *e*-*h* pair. The excitations containing two or more pairs and the polarization produced by the surrounding ions are taken into account by means of the effective screening in the Coulomb interaction, $\epsilon(\mathbf{r}-\mathbf{r}')$.

In the Hartree-Fock formulation of the exciton problem adopted here the dielectric constant is introduced phenomenologically without any distinction between the Coulomb (direct) and exchange terms. On the other hand, in the many-body formulation in terms of the Bethe-Salpeter equation,[25] the exchange term appears unscreened in the *GW* approximation. Indeed, Rohling and Louie[26] have calculated the exciton fine structure in hydrogenated Si clusters with an unscreened exchange interaction. However, in the EMA theory of the exciton in bulk semiconductors it was shown[27,28] earlier that only the short-range part of the *e*-*h* exchange interaction remains unscreened, but the long-range part is screened. Recently, Franceschetti *et al.*[29] have argued that in a QD the exchange interaction [Eq. (9)] contains an important long-range part that needs to be screened. Indeed, they found that within their pseudopotential theory, unscreened exchange leads to an excitonic splitting much larger than the experimental values. As explained below, we reach a similar conclusion in the TB model. There is, of course, no basic controversy over the screening of the Coulomb term. We assume a uniform static dielectric constant, with a size dependence roughly following Ref. 30. As for the screening of the exchange term, we carried out two different calculations: (i) completely unscreened and (ii) unscreened up to the nearest neighbors but screened beyond. A comparison of our results with the experimental Stokes shift data clearly favors the second choice.

TABLE III. On-site unscreened Coulomb and exchange integrals for cation (anion) in eV.

| | $u^{\Gamma_6}$ | $u^{\Gamma_8}$ |
|---|---|---|
| $u^{\Gamma_6}$ | 13(6.5) | 1(0.5) |
| $u^{\Gamma_8}$ | 1(0.5) | 13(6.5) |

The TB approach aims to give an appealing physical description with only a few adjustable parameters. Following this spirit we try to reduce the number of integrals by means of some reasonable approximations. Let us take a generic integral in the local spin-coupled basis that appears when Eqs. (8) and (9) are expanded in terms of the QD states given in Eq. (1),

$$\left\langle u_{m_1}^{k_1}(\mathbf{r}-\mathbf{R}_1)u_{m_2}^{k_2}(\mathbf{r}'-\mathbf{R}_2)\left|\frac{V(\mathbf{r}-\mathbf{r}')}{\epsilon(\mathbf{r}-\mathbf{r}')}\right|u_{m_3}^{k_3}(\mathbf{r}'-\mathbf{R}_3) \times u_{m_4}^{k_4}(\mathbf{r}-\mathbf{R}_4)\right\rangle. \tag{10}$$

First, we retain only integrals involving up to two distinct orbitals by setting the subscripts as either (i) $3=2$ and $4=1$ or (ii) $3=1$ and $4=2$. The two choices correspond to the Coulomb and exchange integrals, respectively. Second, if $\mathbf{R}_2 \neq \mathbf{R}_1$ the Coulomb integral is approximated by the monopole-monopole term: $V(|\mathbf{R}_2-\mathbf{R}_1|)$. Finally, the on-site Coulomb integrals are simplified: $U_{s*s*}=U_{s*p}=U_{s*s}=0$ and $U_{ss}=U_{pp}=U_{sp}=U$, but $U$ takes different values for the cation and the anion. These Coulomb integrals are treated as phenomenological parameters but follow qualitatively Ref. 13 for the on-site Coulomb and exchange integral values.

The assumed on-site Coulomb and exchange integrals are given in Table III. We have checked, however, that the final results are not strongly dependent on these integrals when the diagonal values change by 1 eV. Finally, the Coulomb integrals are screened in the Coulomb Hamiltonian; they are left unscreened up to the nearest neighbors (primitive cell of the zinc-blende crystal) in the exchange term and screened otherwise. The on-site screening factor is taken to be 0.4 and 0.5 for cations and anions, respectively. The nearest-neighbor exchange integrals, important only in the exchange Hamiltonian, are assumed to be a tenth of the unscreened on-site integrals.

The exciton Hamiltonian in Eq. (7) is treated by a configuration-interaction-like method where we take as many *e-h* pair states as necessary to get convergence in the final energies and energy differences. The size of the exciton space is not *a priori* fixed. For the high-energy transitions, it is adequate to evaluate the average value of the Coulomb term and we take as many as 48–50 valence states and 44–46 conduction states, depending on the QD size. On the other hand, the low-energy fine structure requires a diagonalization of the full *e-h* Hamiltonian including the exchange term and computer time restrictions appear; the number of valence and conduction states needed to reach convergence is up to 18 and 14, respectively. As in previous works[12,13] the numerical convergence is faster for the energy differences than for the energy levels. The fine-structure levels are fixed when the energy difference of the first excited level has converged to within 0.1 meV. The highest levels analyzed in the fine structure present convergence to within 1 meV.

## III. RESULTS

### A. Fine structure

An early analysis of the band-edge exciton states within the EMA was reported by Efros *et al.*;[3] it has been used as a guideline in the TB[13] and pseudopotential[12] calculations. In the spherical EMA the eightfold multiplet originating from the fourfold highest valence and the twofold lowest conduction levels is split by the electron-hole interaction into a fivefold passive multiplet and a threefold active triplet. Within our TB model, the $T_d$ symmetry analysis leads to three exciton levels,

$$\Gamma_8^v \times \Gamma_6^c = \Gamma_3^{vc} + \Gamma_4^{vc} + \Gamma_5^{vc}.$$

If we call $H^Z$ the exciton Hamiltonian that presents the zinc-blende symmetry (i.e., the TB Hamiltonian $H_0$ plus the Coulomb and exchange interaction terms but no crystal field), then eigenenergies of these states can be written in terms of the matrix elements of $H^Z$ as

$$\begin{aligned} E_3 &= \tfrac{1}{2} H^Z_{3/2,-1/2;3/2,-1/2} - H^Z_{3/2,-1/2;-3/2,1/2} \\ &\quad + \tfrac{1}{2} H^Z_{-3/2,1/2;-3/2,1/2}, \\ E_4 &= \tfrac{1}{2} H^Z_{-1/2,-1/2;-1/2,-1/2} + H^Z_{-1/2,-1/2;1/2,1/2} \\ &\quad + \tfrac{1}{2} H^Z_{1/2,1/2;1/2,1/2}, \\ E_5 &= E_3 + 2H^Z_{3/2,-1/2;-3/2,1/2}, \end{aligned} \tag{11}$$

where for the sake of simplicity $H^Z_{m1,m2;m3,m4}$ stands for $\langle v^8_{m1}, c^6_{m2} | H^Z | v^8_{m3}, c^6_{m4} \rangle$. We compare now the analytical result in Eq. (11) with the numerical diagonalization of $H^Z$, which allows us to identify the symmetry of the states. The resulting order for any size is $E_3 < E_4 < E_5$, but $E_3$ and $E_4$ are almost degenerate.

The introduction of the crystal-field term reduces the symmetry to $C_{3v}$, leading to a splitting of the previously threefold degenerate levels $\Gamma_4^{vc}$ and $\Gamma_5^{vc}$. From the $T_d$ to $C_{3v}$ compatibility table[20] the $\Gamma_4^{vc}$ level is split into $\Gamma_2^{vc} + \Gamma_3^{vc}$ and $\Gamma_5^{vc}$ level into $\Gamma_1^{vc} + \Gamma_3^{vc}$. From this result we can deduce that the $\Gamma_2^{vc}$ singlet is symmetry-forbidden. It is important to know if the rest of these first eight levels are truly active. To elucidate this question we first project the states obtained from the diagonalization of $H^Z + H_{\mathrm{CF}}$ onto the eight states obtained from $H^Z$. It is known from group theory that only the $\Gamma_5^{vc}$ levels can be optically active so we only need the projection of the states obtained from the complete Hamiltonian onto these $\Gamma_5^{vc}$ active states.

TABLE IV. Fine-structure analysis of the first eight states of the $D = 40.22$ Å quantum QD. The first column shows the energies and the corresponding symmetry (in parentheses). The second column shows the relative fraction of $\Gamma_5^{vc}$ state (see text) and in the third column we give the numerically calculated oscillator strength (in arbitrary units).

| Energy (eV) | $\Gamma_5$ fraction | Oscillator strength |
|---|---|---|
| 2.3076 (3) | 0.0 | 0.0 |
| 2.3129 (3) | 52.47 | 1.58 |
| 2.3283 (2) | 0.0 | 0.0 |
| 2.3307 (3) | 43.52 | 1.02 |
| 2.3351 (3) | 97.29 | 1.04 |

The resulting projections show that the lowest state, a doublet, is not active and the two other doublets and the $\Gamma_1$ singlet are symmetry-permitted. However, even with this analysis it is not enough to conclude that the first doublet is forbidden; it could have other contributions from active states of higher energy. We compute then the oscillator strength (see the Appendix) for the five different levels. In Table IV the detailed results of this analysis are shown for a QD of size $D = 40.22$ Å. This allows us to confirm that the first doublet is optically forbbiden even when 18 valence and 16 conduction states are included to build the excitonic matrix. This result agrees with the EMA[3] and pseudopotential[12] calculations, but not with that of Ref. 13. We believe this contradiction with the previous TB calculation arises from the different procedures followed. We include the spin-orbit interaction from the beginning and deduce the full single-particle spectrum. Leung *et al.* considered this term perturbatively at the same level as the Coulomb interaction, applied to a small number of band-edge states extracted by using a Lanczos algorithm.

Let us recall that an analysis of our one-particle spectrum indicates that instead of a fourfold degenerate valence level it is more appropriate to consider two fourfold valence levels that are very close in energy (see Table II). Thus a symmetry analysis of the fine structure must take into account the first 16 exciton states instead of 8. The analysis of this very restricted set of states gives results that are very close to the final values when the numerical convergence is reached. The 16 exciton states are structured in general as two repeated eightfold multiplets. It is remarkable, however, that the biggest QD presents a special behavior when convergence is reached. In this case the degeneracy pattern of the 16 states is 2222121121 instead of the 2212122121 for the smaller sizes.

The resonant Stokes shift is normally compared with the energy difference between the lowest optically active

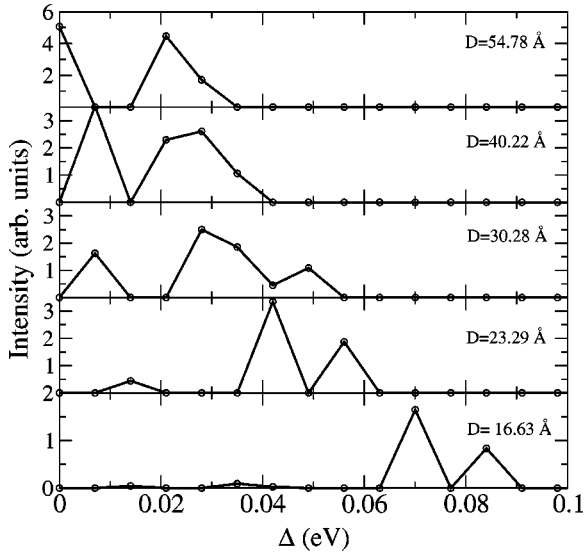


FIG. 3. Fine-structure optical absorption spectra for several sizes of CdSe nanocrystals. The evolution of the first peak, associated with the Stokes shift, shows a singular behavior for the smallest of the QD's studied here. The size of the two lowest peaks is negligible compared with the next peak. This behavior may be related to the sudden increase of the measured Stokes shift in small-size QD's (see text).

(bright) and the lowest forbidden (dark) exciton states.[3,12,13] In Fig. 3 the calculated absorption spectra for several QD's are shown. We identify the first peak with the position of the first allowed level. The size dependence of the resulting resonant Stokes shift is shown in Fig. 4 and compared with the available experimental data. There is an overall agreement between the theoretical predictions and experimental data. The data of the smallest QD's considered here present, however, a peculiar behavior. The intensity in the two smallest QD's in Fig. 3 shows that the first transition goes to zero and also that an additional splitting of the first active state appears and eventually could produce an unclear definition of the theoretical Stokes shift. For example, if we associate the mean value of the two smallest peaks of the smallest QD studied to the Stokes shift we obtain 28.1 meV. On the other hand, one could be tempted to say that the shift measured corresponds to the energy difference between the first of the big peaks and the dark level. This feature might explain why the experimental values grow so much with decreasing sizes. Another interesting feature is the distribution of oscillator strength in the EMA. It was shown that in spherical and elliptical shape QD's the oscillator strength of the first active state, $\pm 1^L$, relative to that of the $0^U$ goes to zero for decreasing QD radius and grows with increasing QD size.[3] We find the same qualitative feature in our model but due to the existence of more than three active states a full comparison is not possible. In Fig. 4 there is also another interesting aspect concerning the results for two QD's with similar sizes, 30.28 and 31.6 Å in diameter. In fact, the difference is due to one shell of cadmium atoms. It can be seen that the shift increases for the bigger QD, which is opposite to the overall trend of decreasing shift with increasing size. We associate this surprising behavior with the relative number of dangling bonds in the surface of the QD. This perhaps account for a similar behavior of the experimental Stokes shifts. Finally, we have also carried out calculations assuming a completely unscreened *e-h* exchange interaction; the results are shown as open triangles connected by dotted lines. The Stokes shift is slightly enhanced in small QD's, improving the agreement with experimental data. However, in large QD's, the enhancement is too large and does not correctly extrapolate toward the bulk exciton splitting. We therefore conclude that, at least from a phenomenological point of view, it is necessary to screen the exchange interaction beyond the first neighbor, in qualitative agreement with Ref. 29.

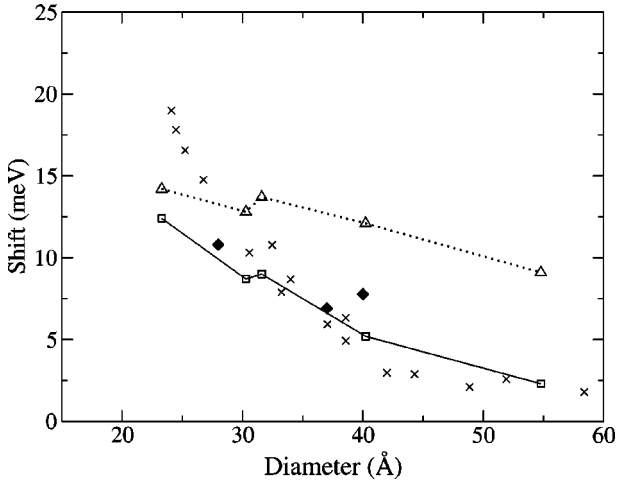


FIG. 4. Resonant Stokes shift obtained from the energy position of the lowest energy peak in Fig. 3 (squares), compared with the experimental measurements from Efros *et al.* (Ref. 3) (crosses) and Chamarro *et al.* (Ref. 5) (closed diamonds). The triangles connected by dotted lines correspond to a completely unscreened *e-h* exchange interaction, while the squares connected by solid lines correspond to a finite screening beyond the first neighbors.

The interpretation of the Stokes shift of the nonresonant photoluminescence seems less unambiguous. According to Efros *et al.*, it would correspond to the energy difference between a higher active state and the lowest active one, while Chamarro *et al.* consider it to be the energy difference between a higher active state and the dark ground state. We have adopted the latter point of view in presenting the experimental data in Fig. 5. In the TB model we analyze the first 16 exciton states. The resulting excited levels, referred to the dark ground state, are shown in Fig. 5 along with their relative intensities. The size dependence is expressed in terms of the exciton ground state energy as the abscissa. One difficulty of the comparison between theory and experiment here is that there is no easy way to establish a one-to-one relation between our single-QD computed values and the measured points. First, the presence of several levels close in energy should be considered. Also, the size distribution of the QD's must be considered as was pointed out by Efros et al.[3] In Fig. 5 we show again the results for two QD's of similar size as in Fig. 4. Note the significant differences between them, in particular, the increase in energy of transition as well as the shifting of the absorption intensities to higher

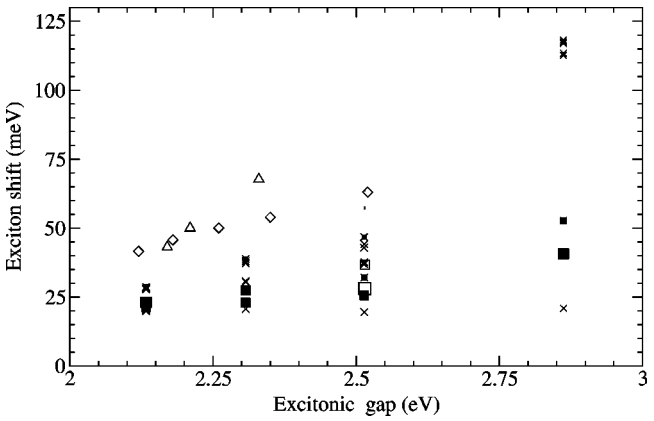


FIG. 5. The size dependence of the first excitonic levels (we have omitted the first active level, considered before). Note that the abscissa is the exciton ground-state energy instead of the QD size. All the levels are indicated by a cross. The allowed transitions present additionally a closed square whose size (area) is proportional to the absorption intensity. The open squares stand for the $D=31.60$ Å case. We also show the measured values of the nonresonant Stokes shifts from Norris and Bawendi (Ref. 8) (open diamonds) and Chamarro *et al.* (Ref. 5) (open triangles).

energies. Finally, let us mention that, as expected, an unscreened *e-h* exchange leads to larger theoretical values, yielding better agreement with experimental data. However, a fit to the resonant Stokes shift data seems more significant. We have therefore retained the screening of the exchange beyond the first neighbor.

### B. High-energy transitions

The high-energy transitions are also analyzed in detail. First the absorption coefficient is computed following a simplified procedure (see the Appendix). Considering the energy scale involved, we neglect the exchange term in the interaction Hamiltonian and treat the Coulomb term as a first-order perturbation. We identify by inspection the major peaks; in Fig. 6 we show the optical absorption spectra for several QD sizes. We deduce the symmetries of the valence and conduction states concerned as well as their relative weights when more than one valence-to-conduction transition is involved. Table V shows the results for the $D=40.22$ Å QD. This analysis is done first for the smaller QD, where the peaks are well separated and clearly distinguishable. Then the same analysis is performed for the bigger QD's, where we try to follow the size evolution of the peaks. The existence of level crossing makes it difficult to clearly identify these peaks. For example, the second and third peaks for the two smallest QD's are $\Gamma_8^v \rightarrow \Gamma_7^c$ and $\Gamma_8^v \rightarrow \Gamma_8^c$ transitions, respectively. The two biggest QD's present a reversed order. The evolution of the higher peaks is more complicated, due to the mixing of different transitions into each of the peaks.

The peaks are not immediately identified with the experimental transitions but instead in some cases we find it appropriate to group several peaks in the same transition. The results are summarized in Fig. 7.

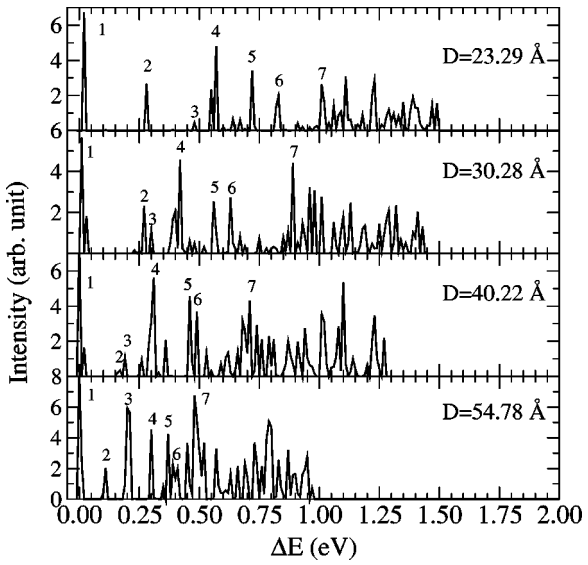


FIG. 6. The size dependence of the absorption coefficient $\alpha(E)$ at high energies. The energy is measured from the ''band gap'' in each case.

## IV. SUMMARY

We present a unified picture of the optical properties of spherical CdSe nanocrystals based on the $sp^3s^*$TB model including the spin-orbit interaction that describes the main features of the bulk semiconductor band structure. Our group-theoretical method has allowed us to deduce the full one-particle spectra with symmetry-classified eigenstates for crystallite sizes up to 55 Å in diameter. The dangling bonds were passivated by hydrogen atoms. The degree of saturation of the dangling bonds strongly influences the electronic properties of the QD's due to the presence of surface states near the band edges. The bond lengths from the outermost cation or anion to hydrogen were used to study this effect. The final choice of the bond lengths removes the surfaces states completely and optimizes the Stokes shift. The wurtzite structure of CdSe is treated as usual by introducing a crystal-field term, reducing the symmetry from $T_d$ to $C_{3v}$.

With the single-particle states in hand, the exciton states are written in terms of Slater determinants, limiting us to the

TABLE V. High energy transitions for the $D=40.22$ Å QD. The symmetry structure of the seven first peaks are shown. If more than one transition is involved the two most important fractions are written.

| Peak number | Valence-conduction state | Fraction |
|---|---|---|
| 1 | 8-6 | 1 |
| 2 | 8-6 | 1 |
| 3 | 7-6 | 1 |
| 4 | 8-8 (8-7) | 0.65 (0.34) |
| 5 | 7-6 (8-6) | 0.99 (0.01) |
| 6 | 8-8 (6-7) | 0.77 (0.17) |
| 7 | 6-7 (6-8) | 0.75 (0.25) |

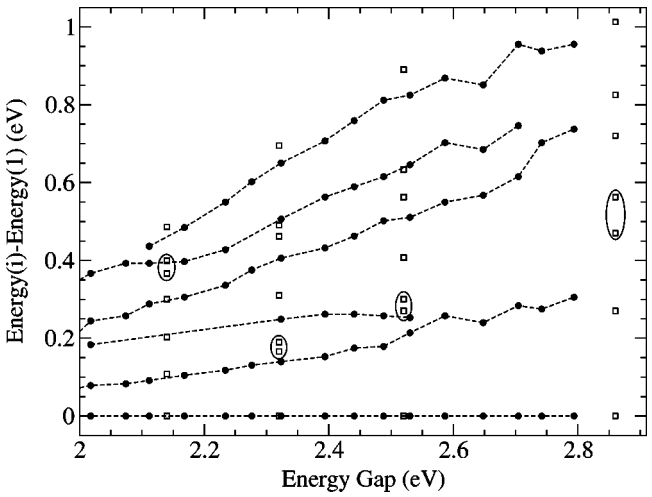


FIG. 7. High-energy excitonic transition energies are plotted against the the excitonic gap (open squares) and compared with the experimental data from Ref. 8 (closed circles). The encircled points suggest a probable merger.

subspace of single electron-hole pair excitations. The electron-hole interaction including both the direct (Coulomb) and exchange terms is taken into account. In order to derive the fine structure of low-energy excitations, the full exciton Hamiltonian is diagonalized in a subspace of progressively increasing size, with as many valence and conduction states as necessary to reach convergence. The relative electric-dipole transition probabilities of the exciton fine-structure components were calculated numerically and checked against a symmetry analysis using a restricted subspace. The ground state is found to be forbidden in all cases, in agreement with the EMA and pseudopotential calculations, but in contradiction with the previous TB calculations,[13] based on a Lanczos algorithm and a perturbative treatment of the spin-orbit interaction. The energy of the first allowed peak in the theoretical absorption spectrum yields the resonant Stokes shift of the photoluminescence. The theoretical values agree with the measured data except for the very small QD's. The origin of the discrepancy is probably the increasing importance of the surface effects in the QD's when their size decreases. Indeed it can be seen that for the small QD's ($D < 20\,\text{Å}$) there are as many or more dangling bonds as atoms. Recently Leung and Whaley[14] studied the influence of the surface for small QD's and found an increase of the Stokes shift after optimized surface relaxation.

We have also investigated the nonresonant Stokes shift, which is associated with allowed states lying above the first bright level. The theoretical results are systematically smaller than the measured values. There are probably several reasons for the discrepancy. First we have not included the phonons in our model, which seem to be important in the analysis of the experimental data (see Ref. 3 and references therein). Also our results are given for each QD individually; we have not taken into account the size distribution of the sample that apparently enhances the theoretical shift.[3] Finally, from a theoretical point of view, we find that the exciton fine structure depends rather strongly on the surface conditions: both the surface-to-volume ratio and the degree of saturation of the dangling bonds. Also the geometry (crystal structure or sample shape) plays an important role, as suggested by the increase of the Stokes shifts with increasing crystal field.

The high-energy excitonic transitions have been also studied. The comparison of the theoretical results with the available experimental data shows reasonable agreement.

## ACKNOWLEDGMENTS

We wish to thank M. Chamarro for stimulating and fruitful discussions.

## APPENDIX: ABSORPTION COEFFICIENT

The absorption coefficient $\alpha$ is related to $\epsilon_2, \alpha \sim \omega \epsilon_2$,[31] where

$$\epsilon_2 \sim \frac{1}{E^2} \sum_f |M_{fg}|^2 \delta(E - E_{fg}), \tag{A1}$$

where $|M_{fg}|^2$ is squared transition dipole matrix given by[13]

$$M_{fg} = \langle f|[\mathbf{r}, H]|g\rangle = -E_f \sum_{vc} C^*_{vc} \langle c|\mathbf{r}|v\rangle, \tag{A2}$$

where $E_f$ is the exciton energy referred to the band gap $E_g$. It is then easy to check that the absorption coefficient can be written, in appropriate units as

$$\alpha(E) \sim \sum_f E_f^{-1} |M_{fg}|^2 \delta(E - E_{fg}). \tag{A3}$$

The dipole matrix $\langle e|\mathbf{r}|v\rangle$ is written in terms of the one particle states in Eq. (1) as

$$\langle e|\mathbf{r}|v\rangle = \sum_{R_s,k,m,R_{s'},k',m'} C^{c*}_{R_{s'},k',m'} C^{v}_{R_s,k,m} [\mathbf{R}_s \delta_{ss'} \delta_{kk'} \delta_{mm'} + \langle u^{k_s'}_{m_s'}(\mathbf{r} - \mathbf{R}_{s'})|\, \delta\mathbf{r}_s |u^{k_s}_{m_s}(\mathbf{r} - \mathbf{R}_s)\rangle], \tag{A4}$$

where $\delta\mathbf{r}_s = \mathbf{r} - \mathbf{R}_s$. We follow the prescription given in Ref. 13 for the nonzero elements. The spin flips are forbidden in optical transitions and we account for that by means of the explicit expressions for the on-site and nearest-neighbor dipole matrix elements:

$$\begin{aligned}
\langle u^{6s*}_{-1/2}|\, \delta\mathbf{r}_s |u^{7p}_{-1/2}\rangle &= i\sqrt{\frac{1}{3}} d_1 \mathbf{e}_z, \\
\langle u^{6s*}_{-1/2}|\, \delta\mathbf{r}_s |u^{8p}_{-3/2}\rangle &= i\sqrt{\frac{2}{3}} d_1 \mathbf{e}_z, \\
\langle u^{6s*}_{+1/2}|\, \delta\mathbf{r}_s |u^{7p}_{+1/2}\rangle &= i\sqrt{\frac{1}{3}} d_1 \mathbf{e}_z, \\
\langle u^{6s*}_{-1/2}|\, \delta\mathbf{r}_s |u^{8p}_{+3/2}\rangle &= i\sqrt{\frac{2}{3}} d_1 \mathbf{e}_z,
\end{aligned} \tag{A5}$$

and

$$\langle u^{k'}_{m'}|\, \delta\mathbf{r}_s |u^{k}_{m}\rangle = 4 d_2 \delta_{kk'} \delta_{mm'} \mathbf{e}_z, \tag{A6}$$

when $u_m^{k'}$, and $u_m^k$ belong to nearest-neighbors atoms. In the last case the $u_m^k$ are only those originated by $s$, $p_x, p_y, p_z$ atomic orbitals. For $d_1$ and $d_2$ we take the numerical values given in Ref. 13 even though we are only interested in the relative values of the intensity.

The high-energy transitions have been analyzed by means of a simplified Hamiltonian where the exchange term has been neglected. Additionally we take only the diagonal correction of the Coulomb term: The expression in Eq. (A2) is simplified to ($|f\rangle = |vc\rangle$),

$$M_{fg} = \langle f|[\mathbf{r}, H]|g\rangle = -(\epsilon_c - \epsilon_v - J_{vc})\langle c|\mathbf{r}|v\rangle. \quad \text{(A7)}$$


[1] D. Bimberg, M. Grundmann, and N. N. Ledentsov, *Quantum Dot Heterostructures* (Wiley, Chichester, 1998).

[2] C. B. Murray, D. J. Norris, and M. G. Bawendi, J. Am. Chem. Soc. **115**, 8706 (1993).

[3] AI. L. Efros, M. Rosen, M. Kuno, M. Nirmal, D. J. Norris, and M. G. Bawendi, Phys. Rev. B **54**, 4843 (1996).

[4] M. Chamarro, C. Gourdon, P. Lavallard, O. Lublinskaya, and A. I. Ekimov, Phys. Rev. B **53**, 1336 (1996).

[5] M. Chamarro, M. Dib, C. Gourdon, P. Lavallard, O. Lublinskaya, and A. I. Ekimov, in *Advances in Microcrystalline and Nanocrystalline Semiconductors—1996*, edited by R. W. Collins, P. M. Fauchet, I. Shimizu, J.-C. Vial, T. Shimada, and A. P. Alisivatos, Mater. Res. Soc. Symp. Proc. No. **452** (Material Research Society, Pittsburgh, 1997), p. 341.

[6] M. Chamarro, M. Dib, V. Voliotis, A. Filoramo, P. Roussignol, T. Gacoin, J. P. Boilot, C. Delerue, G. Allan, and M. Lannoo, Phys. Rev. B **57**, 3729 (1998).

[7] W. Hoheisel, V. L. Colvin, C. S. Johnson, and A. P. Alisivatos, J. Chem. Phys. **101**, 8455 (1994).

[8] D. J. Norris and M. G. Bawendi, Phys. Rev. B **53**, 16 338 (1996).

[9] J. Li and J. B. Xia, Phys. Rev. B **61**, 15 880 (2000).

[10] U. E. H. Laheld and G. T. Einevoll, Phys. Rev. B **55**, 5184 (1997).

[11] L. W. Wang and A. Zunger, J. Chem. Phys. **34**, 6439 (1998).

[12] A. Franceschetti, H. Fu, L. W. Wan, and A. Zunger, Phys. Rev. B **60**, 1819 (1999).

[13] K. Leung, S. Pockrant, and K. B. Whaley, Phys. Rev. B **57**, 12291 (1998).

[14] K. Leung and K. B. Whaley, J. Chem. Phys. **110**, 11 012 (1999).

[15] AI. L. Efros, Phys. Rev. B **46**, 7448 (1992).

[16] P. Vogl, H. P. Hjalmarson, and J. D. Dow, J. Phys. Chem. Solids **44**, 365 (1983).

[17] V. Albe, C. Jouanin, and D. Bertho, Phys. Rev. B **58**, 4713 (1998).

[18] A. Kobayashi, O. F. Sankey, and J. D. Dow, Phys. Rev. B **25**, 6367 (1982).

[19] J. Pérez-Conde and A. K. Bhattacharjee, Solid State Commun. **110**, 259 (1999).

[20] G. F. Koster, J. O. Dimmock, R. G. Wheeler, and H. Statz, *Properties of the Thirty-Two Point Groups* (MIT Press, Cambridge, MA, 1963).

[21] P. E. Lippens and M. Lannoo, Phys. Rev. B **41**, 6079 (1990).

[22] T. Richard, P. Lefevre, H. Mathieu, and J. Allegre, Phys. Rev. B **53**, 7287 (1996).

[23] See, for example, A. R. Edmonds, *Angular Momentum in Quantum Mechanics* (Princeton University Press, Princeton, 1960).

[24] S. V. Nair, L. M. Ramaniah, and K. C. Rustagi, Phys. Rev. B **45**, 5969 (1992).

[25] L. J. Sham and T. M. Rice, Phys. Rev. **144**, 708 (1966).

[26] M. Rohling and S. G. Louie, Phys. Rev. Lett. **80**, 3320 (1998).

[27] U. Rösler and H. R. Trebin, Phys. Rev. B **23**, 1961 (1981).

[28] V. A. Kiselev and A. G. Zhilich, Fiz. Tverd. Tela (Leningrad) **14**, 1438 (1972) [Sov. Phys. Solid State **14**, 1233 (1972)].

[29] A. Franceschetti, L. W. Wan, H. Fu, and A. Zunger, Phys. Rev. B **58**, R13 367 (1998).

[30] L. W. Wang and A. Zunger, Phys. Rev. B **53**, 9579 (1996).

[31] P. Y. Yu and M. Cardona, *Fundamental of Semiconductors* (Springer-Verlag, Berlin, 1996).